http://dx.doi.org/10.17159/2411-9717/2015/v115n12a6

Mechanical behaviour of pack carburized AISI 316L austenitic stainless steel

by D.E.P. Klenam*†, C. Polese†‡, L.H. Chown*†, S. Kwofie‡‡, and L.A. Cornish*†

Synopsis

The effect of surface hardening by pack carburizing on the mechanical properties of AISI 316L steel was studied. Pack carburizing with 60 wt% $BaCO_3$, 30 wt% activated carbon, and 10 wt% sodium chloride was carried out at 450, 550, 650, 700, and 750°C for 24 hours and the specimens were furnace-cooled. Tensile, impact, hardness, and fatigue tests were conducted, and SEM and was used to characterize the specimens.

The ultimate tensile strength of the as-received steel was similar to specimens carburized at 450 and 550°C (approx. 650 MPa), but decreased from 638 to 603 MPa with further increase in carburizing temperature from 650 to 750°C.

Hardness profiles of the specimens treated at 450°C and 550°C were similar to the as-received steel, at approximately 250 $HV_{0.5}$. Typical case hardening profiles were obtained for specimens carburized at 650, 700, and 750°C.

The number of cycles to failure (N) of the as-received specimens was close to 60 000, which was similar to those carburized from 450 to 650°C. Further increase in carburizing temperature decreased the cycles to failure to approximately 25 000 (700°C) and 7000 cycles (750°C).

Crack initiation was mainly characterized by cleavage (mode I) for all tested carburized and as-received specimens. Specimens carburized at 450, 550, and 650°C also showed secondary cracking. The final rupture zone contained ductile fracture with dimples, and the specimens showed extensive plastic deformation.

Keywords

316L austenitic stainless steel, mechanical behaviour, fractography, pack carburizing.

Introduction

Austenitic stainless steels are widely used for structural applications in the petrochemical, telecommunication, aerospace, and food-processing industries. This is due to their excellent corrosion resistance and good mechanical properties, such as toughness, ductility, and formability (Bain and Griffiths, 1927; Jenkins *et al.* 1937; Zapffe, 1949). However, due to the austenitic structure, these steels have quite low surface hardness and poor wear resistance (Bell, 2002; Fewell *et al.*, 2000). To improve the surface properties, diffusion and thermochemical surface treatment techniques such as carburizing (Agarwal *et al.*, 2007; Fewell *et al.*, 2000), nitriding (Bell, 2002), nitro-carburizing (Renevier *et al.*, 1999) and ion implantation (Liang *et al.*, 2007) have been used, without impairing the corrosion resistance of the steel (Bell, 2002; Renevier *et al.*, 1999). The treatment temperatures were kept below 500°C to prevent the formation of chromium carbides and nitrides, which deplete chromium from the matrix and reduce corrosion resistance (Matula *et al.*, 2001).

Little has been reported on the pack carburizing of austenitic stainless steels and its effects on the mechanical properties. This is probably because pack carburizing of these stainless steels is considered a difficult process, due to the presence of the Cr_2O_3 oxide surface layer (Davis, 1994; Mingolo *et al.*, 2006). The tenacious Cr_2O_3 surface layer serves as an inhibiting barrier and is also self-healing, which contributes to the 'stainless' characteristic of stainless steels. However, it was felt a worthwhile endeavour to ascertain whether this cheaper method could be used. Other forms of carburizing, such as gas and plasma, are normally used for stainless steel rather than pack carburizing, which is more commonly used for medium- and low-carbon steels (Agarwal *et al.*, 2007; Fewell *et al.*, 2000; Renevier *et al.*, 1999). The major parameters that influence carburizing are soaking time, carburizing temperature, and carbon potential (Shewmon, 1963).

As a high proportion of mechanical failures are due to fatigue, extensive research is being done in this area (Akita and Tokaji, 2006). Nucleated fatigue cracks grow into macro-cracks, resulting in catastrophic failures. Initiation of fatigue is a surface phenomenon, and approximately 80% of all engineering

* *School of Chemical and Metallurgical Engineering, University of the Witwatersrand, Johannesburg.*

† *DST-NRF Centre of Excellence in Strong Materials, University of the Witwatersrand, Johannesburg.*

‡ *School of Mechanical, Industrial and Aerospace Engineering, University of the Witwatersrand, Johannesburg.*

‡‡ *Department of Materials Engineering, Kwame Nkrumah University of Science and Technology, Kumasi, Ghana.*

 ISSN 2225-6253. Paper received May 2015 and revised paper received Oct 2015.

failures are due to fatigue, which is a cause for concern in surface-modified structures and components (Berríos *et al.*, 2001; Berríos-Ortíz *et al.*, 2004). Fatigue behaviour of austenitic stainless steels with their surfaces modified by techniques such as plasma carburizing and nitriding, ion implantation, shot peening, and physical vapour deposition of coatings with TiN, CrN and ZrN has been studied by Ceschini and Minak (2008), Fewell *et al.* (2000), Agarwal *et al.* (2007), Azar *et al.* (2010), Berríos *et al.* (2001), Collins *et al.* (1995), Liu *et al.* (2003), Samandi *et al.* (1993), and Berríos-Ortíz *et al.* (2004). Surface hardness, wear resistance, and fatigue strength were improved by most of these techniques (Berríos *et al.*, 2001; Berríos-Ortíz *et al.*, 2004; Ceschini and Minak, 2008). Much work has been done on fatigue in stainless steels, but there is no study on pack carburized austenitic stainless steels.

This research was conducted to study the effects of pack carburizing on the mechanical properties and microstructure of AISI 316L stainless steel, and to ascertain which temperatures in the range of 450 to 750°C would provide a suitable carburized case.

Experimental procedure

As-rolled AISI 316L stainless steel plates (1000×1000×30 mm) containing 17.1 wt% Cr were purchased and the composition was determined by optical emission spectroscopy (Table I).

Flat tensile specimens (dogbone shaped) were machined from the as-received plate in the longitudinal rolling direction according to ASTM E8. The length of each sample was 60 mm with the gauge length of 7 mm and thickness of 12 mm. The fatigue specimens having continuous curvature were machined according to ASTM STP91-A. The dimensions were: gauge length of 23 mm, radius of curvature of 190 mm, and a thickness of 6 mm. The Charpy V-notch specimens (45°, 2 mm deep notched bar of length of 55 mm and 10×10 mm thick) were machined according to ASTM A370 (ASTM Standards, 2000). The Charpy V-notch specimens were all notched before the carburizing heat treatment was done. All tests were done in triplicate at all carburizing temperatures.

A container with a lid of dimensions 145×80×80 mm was fabricated from mild steel for the carburizing heat treatment. The tensile, fatigue, and Charpy V-notch specimens were pack carburized in the container with 60% $BaCO_3$ (as the energizer), 30% activated charcoal (source of carbon), and 10% NaCl (activator). The carburizing heat treatment was done at temperatures of 450, 550, 650, 700, or 750°C for 24 hours in a Lenton® muffle furnace, followed by furnace cooling.

Tensile tests were performed according to ASTM E8 using a Tinius Olsen® tensile testing machine under a uniaxial load. Fatigue tests were performed according to ASTM STP91-A using an Instron 1342® fatigue testing machine. The testing was performed at a peak stress of 500 MPa with a stress ratio R of 0.1 (where R = minimum peak stress / maximum peak stress), stress range of 1, and a frequency of 7 Hz. The fractured sample was cut for secondary electron imaging of the fractured surfaces using a FEI Nova® NanoSEM 200. Room-temperature Charpy V-notch impact tests were performed on three impact test samples for each carburizing temperature, according to ASTM A370 (ASTM Standards, 2000). All mechanical tests were performed on pack carburized specimens and on as-received specimens for comparison.

Transverse sections of the carburized and tested samples were prepared metallographically to examine the microstructure from the surface to the centre. The final polishing was done using a colloidal silica suspension on satin woven acetate cloth. The polished specimens were chemically etched using 15 ml HCl, 10 ml HNO_3, and 10 ml ethanol for approximately 8 minutes and were then rinsed in alcohol and water. Scanning electron microscopy with EDX was used to study the microstructures of the as-received and the carburized specimens.

Micro-Vickers hardness testing was done on sectioned samples from the surface to the centre of the carburized and as-received steel specimens, using a load of 500 g and a dwell time of 10 seconds. Hardness-depth profiles were then plotted.

Results

Mechanical tests

The effects of carburizing on the ultimate tensile strength (UTS) of AISI 316L steel is shown in Figure 1. Within error, the ultimate tensile strength was unchanged at approximately 651 MPa for carburizing temperatures of 450°C and 550°C, which is marginally higher than the as-received steel (648 MPa). Further increase in temperature caused a sharp decrease in UTS to 638 MPa (650°C), 627 MPa (700°C), and 603 MPa (750°C).

The effect of carburizing temperature on ductility is shown in Figure 2. The total elongation was almost unchanged with increasing temperature up to 650°C (46-45% compared to the as-received 49%) and decreased more sharply above 650°C to 32% at 750°C. An increase in temperature had a stronger effect on decreasing the reduction in area (% RA). The RA after carburizing at 450°C was the same as the as-received at 79%, and dropped to 65% at 650°C and 45% at 750°C.

The impact energy of the as-received AISI 316L steel was 272 J. After carburizing between 450-750°C, the impact energies decreased with increasing temperature, as shown in

Table I

Analysed chemical composition of AISI 316L steel (in wt%)

Element	C	Si	Mn	P	S	Cr	Mo	Ni	Cu	N	Fe
wt%	0.025	0.42	1.00	0.032	0.031	17.12	2.11	10.13	0.449	0.056	bal.

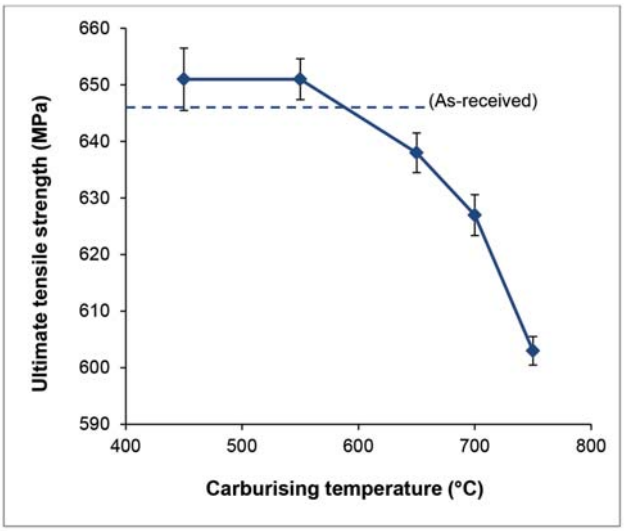

Figure 1 – Effect of carburizing temperature on the ultimate tensile strength of AISI 316L steel

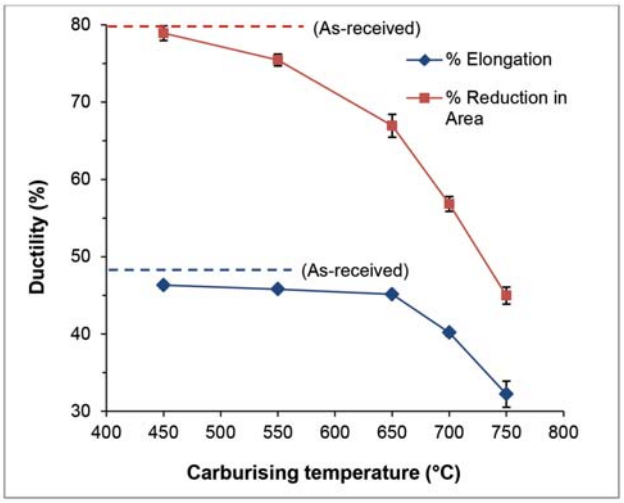

Figure 2 – Effect of carburizing temperature on the ductility of AISI 316L steel

Figure 3, from 257 J at 450°C showing a constant drop in impact energy with increasing carburizing temperature from 550°C (243 J) to 750°C (132 J).

The microhardness measurements for the as-received material varied, with an average surface hardness of 255 $HV_{0.5}$ and a core hardness of 248 $HV_{0.5}$. The specimens that were carburized at 450 and 550°C showed only small differences in hardness between the surface and the core, ranging from 246–255 $HV_{0.5}$, as shown in Figure 4a. Not all the carburizing compound in the case burnt off, thus carburizing was not properly achieved at these two temperatures. However, the surface hardness did increase nominally with increasing temperature for samples carburized at temperatures of 650, 700 and 750°C (Figure 4b). These specimens showed a hardness profile similar to that found in case hardening, with higher hardnesses at the surface and core hardnesses similar to the as-received material. The case depth is related to the amount of carbon diffused inwards

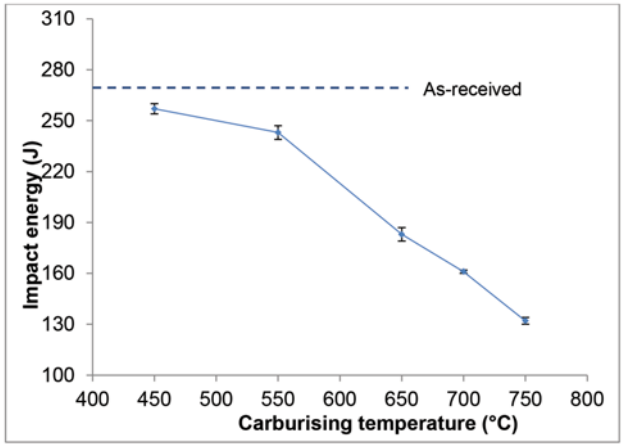

Figure 3 – Effect of carburizing temperature on impact toughness of AISI 316L steel

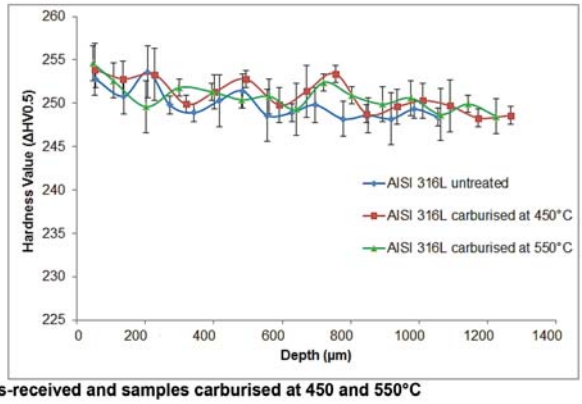

a) As-received and samples carburised at 450 and 550°C

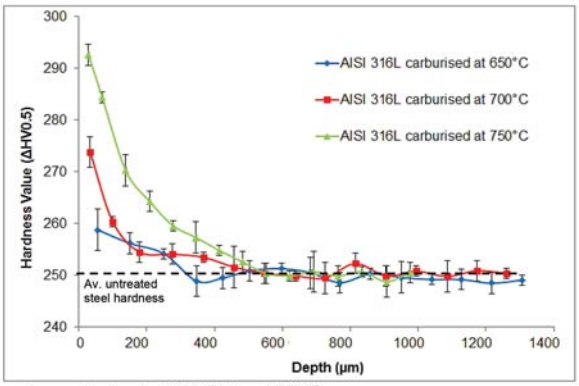

b) Samples carburised at 650, 700 and 750°C

Figure 4 – Effect of carburizing on the depth-hardness profile of AISI 316L

from the surface (Ceschini and Minak, 2008), with the extent of the case indicated by the position where there is a sudden drop in hardness. At 650°C, there was a negligible increase of approximately 5 $HV_{0.5}$ in the hardness of the surface compared to the core; and at 700°C and 750°C the increases were approximately 25 $HV_{0.5}$ and 42 $HV_{0.5}$ respectively.

Microstructures – scanning electron microscopy

The as-received sample had similar microstructures at the surface and core as the sample treated at 550°C (Figures 5a

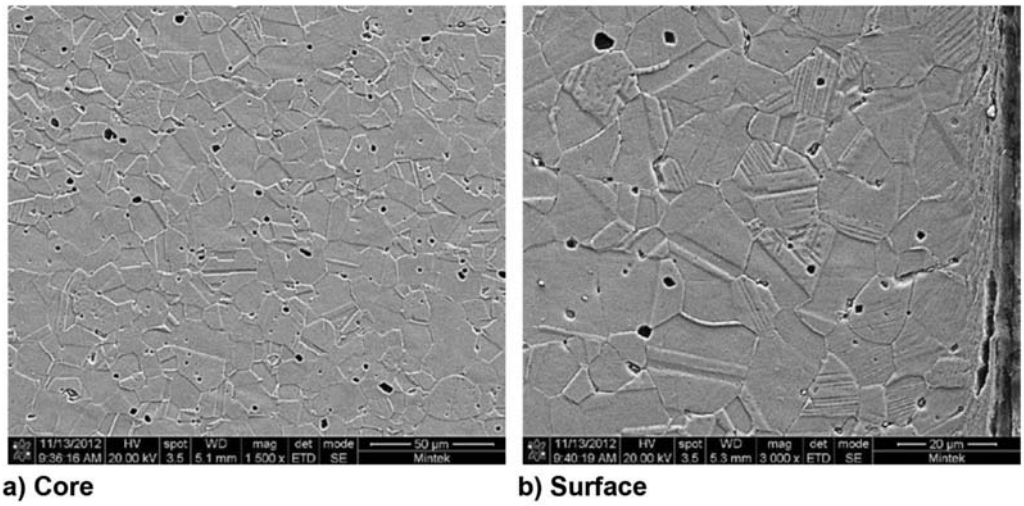

Figure 5 – SEM secondary electron (SE) images of AISI 316L sample carburized at 550°C

and b), showing austenite grains, annealing twins, pores, and some oxides. Figure 5b shows deformation at the sample surface from the rolling process of the as-received steel. There were prominent grain boundaries and etch pits (as found by Fong and Tromans, 1988) throughout the microstructure. No carbides were found by EDX analysis in the specimens treated at 450°C or 550°C. The passive oxide layer on the surface of the sample carburized at 550°C was approximately 8.0 µm thick (Figure 6).

The core and near-surface microstructures of the samples carburized at 700°C also showed austenite grains, annealing twins, slip lines, and pores. Grooved grain boundaries were formed at the core and at the near surface. Intergranular oxidation at the surface of the samples (Figures 7a and b) could be possible, but not at the core since the diffusion of oxygen at temperatures of 550–750°C for 24 hours would be too sluggish for penetration to the core. The grooved grain boundaries at the core could be attributed to the combined effect of sensitization and etching, which produce similar effects in austenitic stainless steels in the ranges of 450–800°C (Agarwal *et al.*, 2007; Ceschini and Minak, 2008). EDX analyses revealed a higher amount of carbides and oxides near the surface compared to the core (Table II). The thin white layer on the surface (Figure 7b) contained calcium and chloride compounds from the carburizing chemicals and the etchant (Figure 7b). There were more slip lines and smaller grains at approx. 50 µm beneath the surface on the near surface (Figure 7b), due to deformation from the finishing rolling.

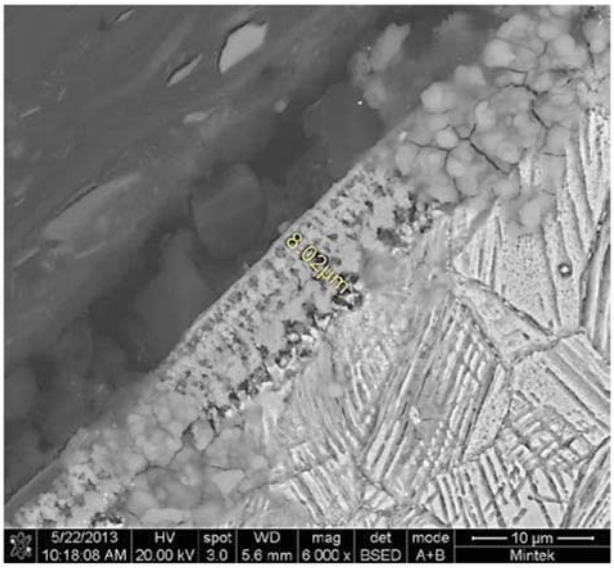

Figure 6 – SEM backscattered electron (BSE) image showing the passive Cr_2O_3 surface layer on the AISI 316L sample carburized at 550°C

Micrographs of samples carburized at 750°C (Figures 8a and b) revealed similar microstructural features to the lower temperature treatments in terms of grain size, carbides, oxides, and voids. Both the core and the near surface underwent grain boundary oxidation. There were more pores on grain and sub-grain boundaries and fewer annealing twins (Figure 8) than at lower carburizing temperatures. The carburized layer was measured as approximately 95–103 µm thick (Figure 9). The grain boundaries became more prominent with increased carburizing temperature.

Fatigue testing and fractography

The effect of carburizing temperature on the fatigue strength of AISI 316L austenitic stainless steel is shown in Figure 10. The fatigue behaviour of samples carburized at 450 to 650°C was similar to the as-received sample, with 50–60 thousand cycles to failure (N). Lower cycles to failure were observed at carburizing temperatures of 700°C (N approx. 26 000), and 750°C (N approx. 8 000), indicating decreasing fatigue resistance of the steel with increase in testing temperature.

Visual inspection of the fractured fatigue surfaces identified ratchet marks and 'thumbnails', indicating regions of slow growth, where the crack was able to maintain its preferred orientation transverse to the applied stress (Roylance, 2001). Macro-examination showed that the edges of the fractured surface were slightly brighter and shiny, a feature known as small fatigue cracks (Ritchie and Lankford,

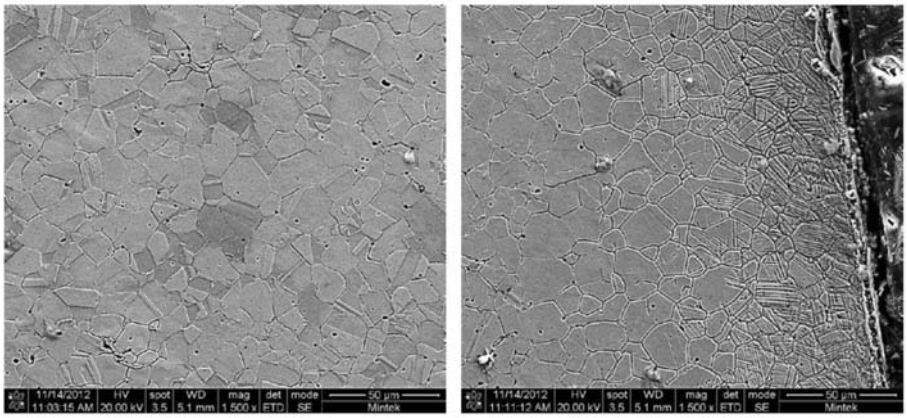

a) Core b) Surface

Figure 7 – SEM SE images of AISI 316L sample carburized at 700°C

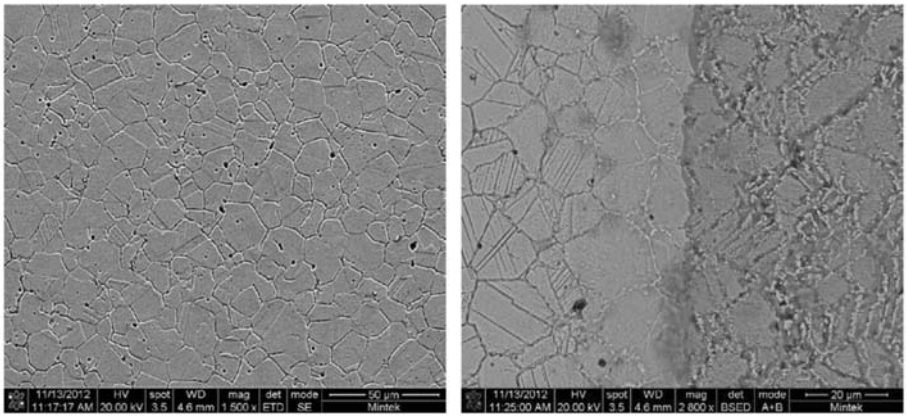

a) Core

b) Surface. BSE of carburized layer, showing penetration along the grain boundaries

Figure 8 – SEM images of AISI 316L samples carburized at 750°C

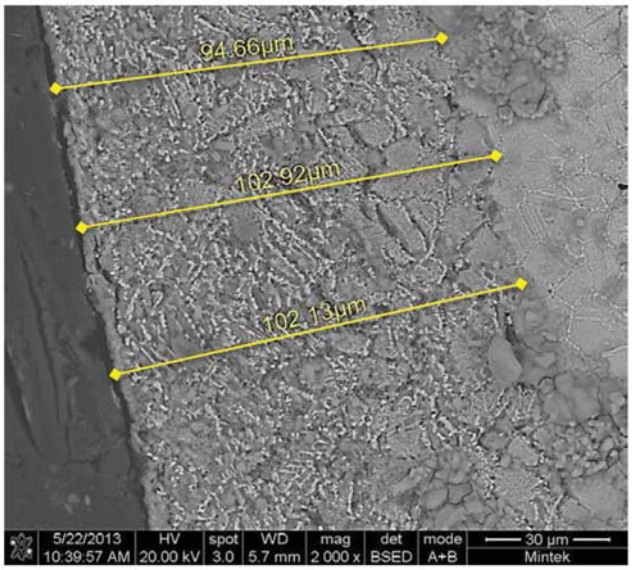

Figure 9 – SEM SE image of the AISI 316L steel carburized at 750ºC, showing the penetration of the carburized layer and oxide layers from the surface towards the core

1986; Agarwal *et al.*, 2007; Ceschini and Minak, 2008;). The fractured surfaces of samples carburised at 450, 550, and 650°C showed more secondary cracking and fatigue pre-

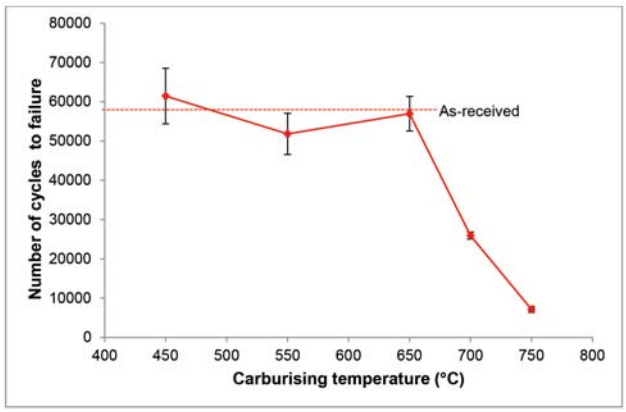

Figure 10 – Effect of carburizing temperature on the fatigue behaviour of AISI 316L steel

cracks along the sides than samples carburized at 700 and 750°C.

SEM examination of the fractured surfaces of all samples showed the crack initiation, propagation, and rupture zones. Cleavage was the characteristic feature of the crack initiation zone (around the edge of the fatigue specimen), with secondary cracking (indicated by an arrow in Figure 11a) for samples carburized at 450°C. The initiation zones showed brittle cleavage, which is a characteristic feature of fatigue crack initiation zones (Fong and Tromans, 1988). The crack propagation zone in Figure 11b shows areas of fatigue striations at regions around the core. The final rupture for the as-received sample was ductile fracture with dimples and micro-voids nucleated within the surface (Figure 11c).

After carburizing at 650°C, the crack initiation stage was characterized by cleavage and dispersed secondary cracking, as shown in Figure 12a. As the cracks propagated, fatigue striations were also found on the fracture surface (Figure 12b). At lower magnification (Figure 12c), the rupture zone showed a step-like pattern. Fractographs of samples carburized at 700 and 750°C (not shown) displayed similar characteristic features to those treated at the lower temperatures.

The fracture surfaces of the Charpy test samples were analysed using SEM. The as-received samples (Figure 13a) and samples carburized at 450°C (Figure 13b) and 550°C showed dimples and microvoid coalescence, which are characteristic of ductile fracture. After carburizing at 650, 700, and 750°C, the fracture surface showed evidence of transgranular brittle fracture. This is shown in Figure 13c for the sample carburized at 750°C.

Discussion

When compared to the as-received sample, carburizing the AISI 316L steel at 450°C slightly improved the ultimate tensile strength, caused marginal decreases in ductility (both elongation and reduction in area), and was detrimental to toughness. At 550°C, the ultimate tensile strength was the same as for 450°C, but the ductility and toughness were lower. Above 550°C, these bulk mechanical properties were compromised, as shown by the incremental loss of ultimate tensile strength, ductility, and toughness with increasing carburization temperature. This was due to the increased coarsening of grain boundary carbides (Fong and Tromans, 1988).

Micrographs of all carburized specimens showed intergranular voids and oxidation along the grain and subgrain boundaries. These defects are potential nucleation sites for cracks (Zavattieri and Espinosa, 2001). Uniaxial tension around these defects could lead to crack opening and the oxides can act as brittle zones (King and Cotterill, 1990), decreasing ductility and toughness of the AISI 316L steel. At

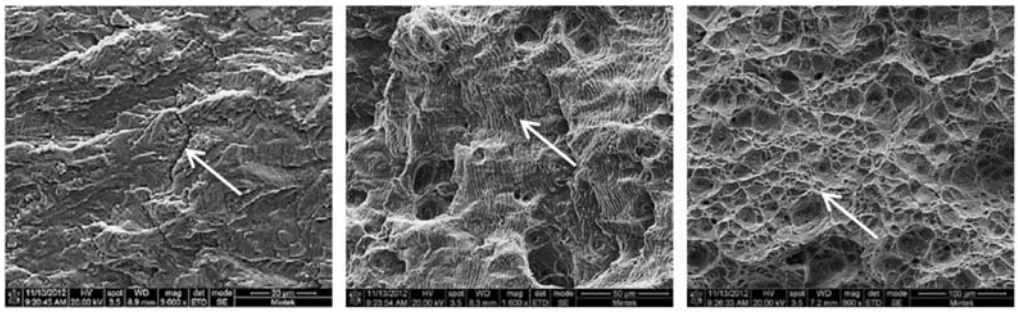

(a) Image taken near the surface of the fatigue specimen where crack was nucleated and initiation zones (with arrow showing secondary cracking)

(b) Image taken approx. 0.3 mm from the surface showing crack propagation, with arrow showing striations

(c) Image taken near the surface where rupture occurred with zones showing ductile fracture and dimples (indicated by arrow)

Figure 11 – SEM SE fractographs of AISI 316L steel carburized at 450°C

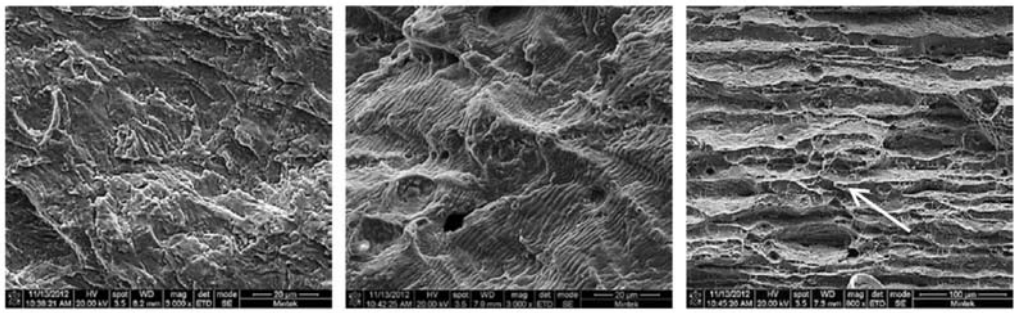

(a) Image taken near the surface of the fatigue specimen where crack was nucleated and initiation zones

(b) Image taken approx. 0.3 mm from the surface showing crack propagation with striations

(c) Image taken near the surface where rupture occurred with zones showing ductile fracture and dimples (indicated by arrow)

Figure 12 – SEM SE fractographs of AISI 316L steel carburized at 650°C

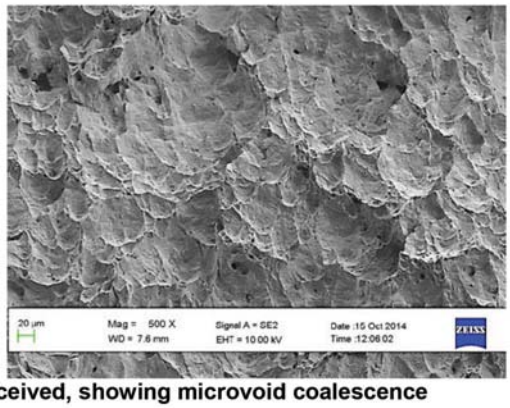

a) As-received, showing microvoid coalescence

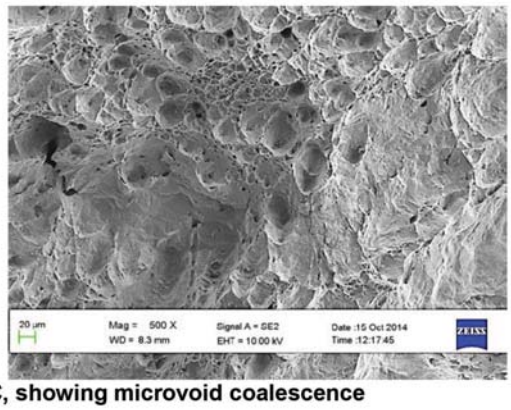

b) 450°C, showing microvoid coalescence

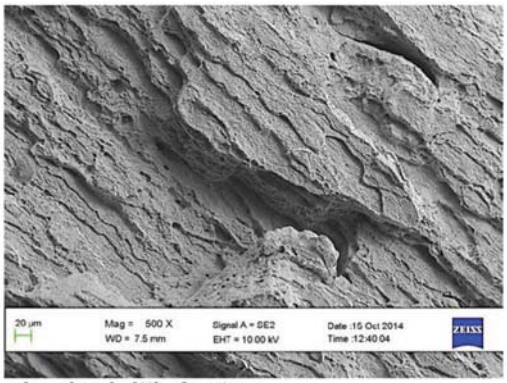

c) 750°C, showing brittle fracture

Figure 13 – SEM SE images taken near the edge of Charpy test specimen fracture surfaces: (a) as-received, (b) carburized at 450°C, (c) carburized at 750°C

450 and 550°C, strengthening from carbon uptake was slightly more beneficial than the negative effect from intergranular oxidation, as seen by the higher tensile strength values.

The amount of carbon that diffused into the steel at 450 and 550°C was too low to significantly increase the surface hardness (Figure 4a). Pores and annealing twins in the austenitic microstructure caused the slight variations in the hardness of these samples and the as-received material. The tenacious, self-healing 8.0 µm thick Cr_2O_3 layer that formed on the steel surface prevented an increase in surface hardness, as these carburizing temperatures and times were insufficient for carbon to diffuse through this inhibitive surface layer. In contrast, the plasma and gas carburizing processes produce permeable oxide layers, which allow enough carbon diffusion into the steel (Renevier *et al.*, 1999; Fewell *et al.*, 2000; Bell, 2002). Thus, high hardness values can be obtained by these processes.

Samples treated at higher temperatures of 650 to 750°C showed hardness profiles similar to those achieved by case hardening, with higher hardness at the surface and core hardness values similar to that of the as-received steel. The highest surface hardness was 294 $HV_{0.5}$ (750°C), which is 18% higher than the core hardness. This indicates a moderate intake of carbon and surface carbon enrichment from the carburizing treatment, which also contributed to the decrease in the ductility and toughness. The presence of twins could also increase the hardness, although the annealing twins were fairly well-distributed throughout the steel and were not concentrated towards the surface. Twin boundaries are known to impede dislocation motion (Lu *et al.*, 2009), which would also contribute to the hardness. However, the main contribution to the higher near-surface hardness was the increasing carbon content from the core to the surface of the stainless steel.

Surface hardnesses of up to 1400 HV have been reported for plasma and gas carburized AISI 316L steel (Fewell *et al.*, 2000; Mingolo *et al.*, 2006). This is substantially higher than the maximum of 294 $HV_{0.5}$ found for the pack carburized samples in this work. The very high surface hardnesses from these carburizing methods can be attributed to high compressive residual stresses from lattice distortion by interstitial carbon, facilitated by the diffusion of carbon through the permeable surface oxide (Fewell *et al.*, 2000; Mingolo *et al.*, 2006).

In XRD spectra, shifts in the austenite peaks to lower diffraction angles indicate compressive residual stresses, which usually improve the mechanical properties (Mingolo *et al.*, 2006). However, the XRD patterns of the carburized samples in this work (not shown) did not display shifts in the austenite peaks. This indicates that there was little interstitial carbon uptake, no substantial change in lattice size occurred, and that negligible compressive residual stresses were induced. A 4% by volume content is required to reliably detect a phase by XRD (Liu, 2006), and the small amounts of carbides and oxides identified by EDX were below this limit. Carbides, which can be detrimental to the corrosion resistance of the AISI 316L steel (Bell, 2002), were present in small amounts in both as-received and carburized samples, as shown by the precipitation at the grain boundaries and within the grains. There was only a very thin observable carburized case.

The number of cycles to failure for the as-received AISI 316L steel and samples carburized from 450–650°C ranged from approximately 52 000 to 61 500 (Figure 10), showing that the fatigue resistance was similar. As the carburizing temperature increased above 650°C, the number of cycles to failure decreased significantly: approximately 26 000 at 700°C and 7 100 at 750°C. Although carburizing at temperatures above 650°C has been reported to lead to stress relief of the compressive stresses and a significant decrease in fatigue strength (Gelfi *et al.*, 2005; Ceschini and Minak, 2008), here the surface had already been removed by the machining of the fatigue samples. Thus, the decrease in the

fatigue strength is more likely to be due to the coarsening of carbides on the grain boundaries at higher carburizing temperatures, which would then have less effect in reducing the initiation and growth of fatigue cracks. Also, the oxides and voids act as imperfections in the material, which could also have been a contributing factor (Lampman, 1997).

The fractured surfaces of the as-received and all of the carburized samples showed cleavage fracture at the initiation stage. SEM examination of the as-received steel fracture surface showed that crack initiation occurred at the surface, which could be attributed to the cyclic and fatigue slip bands (Ceschini and Minak, 2008). Fatigue slip bands, also called persistent slip bands (PSBs), are zones of high cyclic slip activity (Lukáš and Kunz, 2004). The cyclic plastic deformation within PSBs result in surface extrusion and intrusion along the traces of the active slip plane, and fatigue micro-cracks start from these surface intrusions. The initiation of these cracks is also attributed to surface defects such as machining lines, notches, and stress concentration sites (Akita and Bell, 2002; Tokaji, 2006; Agarwal *et al.*, 2007). Cleavage is a Mode I type of fracture, in which shear stresses act parallel to both the crack front and the plane of the crack (Yates and Mohammed, 1996; Tvergaard, 2008; De Freitas *et al.* 2011). The as-received and the carburized samples up to 650°C exhibited acceptable ductility, higher than 65% RA and 45% elongation. Above 650°C, cleavage was observed, which could be attributed to loss in ductility and toughness due to the coarsening of the grain boundary carbides.

Brittle fracture is characterized by quasi-cleavage, low release energy, and minimal plastic deformation (Hull, 1999). These features were absent in the fractured surfaces of the as-received and carburized samples. The increased carburizing temperature enhanced the formation of brittle carbides and grain boundary oxides (Zavattieri and Espinosa, 2001), contributing to the decreased ductility and cleavage of the carburized samples at the crack initiation zones. The fractures originated on the surfaces of the samples, and propagated towards their cores.

The crack propagation zones in all fatigue specimens showed striations, beach marks, and a few secondary cracks, all characteristic features of fatigue failure (Akita and Tokaji, 2006; Bell, 2002). Striations can be attributed to micro-depressions induced in the structure, with the plane normal to the fracture surface, confirming the hollow micro-relief of fatigue striations (Grosskreutz and Waldow, 1963; Ceschini and Minak, 2008). The formation of striations was also due to decohesion along the sub-grain boundaries and possible initiation sites for secondary cracking (Jin-Bo and Chen, 1988; Yang *et al.*, 2008). Secondary cracks are formed by increased stresses due to voids, and occur at sites where there are micro-stress raisers and material defects during crack propagation (Jin-Bo and Chen, 1988). Twinning is caused by continuous mechanical deformation, which leads to discontinuity on the surface of the material, hence creating a site for crack nucleation when stress or strain is applied (James, 1981). Secondary cracks formed along twin bands and propagated below the primary fracture surface (Yang *et al.*, 2008).

The final rupture zones of the as-received and carburized samples showed more ductile dimple rupture than brittle fracture. Ductile dimple rupture occurred by the formation and coalescence of micro-voids along the fracture path. There were faceted patterns within the fractures, suggesting incremental tearing, which could be due to either chemical or microstructural segregation patterns (Gao *et al.*, 1995).

Fractured surfaces of the as-received AISI 316L and samples carburized at 450°C and 550°C showed predominantly ductile fracture, with dimples, microvoid coalescence, and an irregular and fibrous surface, which indicated plastic deformation (Hull, 1999). The dimples on the crack surface are attributed to dislocation movements, which coalesce into grain boundary voids. The carbon diffusion was low and could not cause a major change in the microstructure, nor in the ductility, at these temperatures. At 650°C and above, the fracture appearance was more brittle, with more faceting, which is a characteristic feature of transgranular fracture (Hull, 1999). The Charpy toughness is a bulk material property and the carburizing effect was very shallow, in the order of 100 µm. Therefore, reduced Charpy toughness could not be attributed to the carburizing effect, but rather attributed to the coarsening of grain boundary carbides, which is known to cause a decrease in toughness for austenitic stainless steels (Fong and Tromans, 1988).

The tensile behaviour was more sensitive to carburization than the fatigue behaviour. The tensile and fatigue specimens had different geometries, but this probably did not have a major effect, as the thicknesses were within 1 mm. All test pieces were mixtures of carburized layers and non-carburized cores, and the different proportions of these would have had an effect on mechanical properties. The tensile specimens were slightly thicker (7 mm diameter) than the fatigue specimens (6 mm thickness), and the surface to volume effect of the specimens would have meant that the proportion of the carburized layer of the fatigue specimens was slightly higher, due to their flat, rectangular cross-sections. However, since fatigue is a surface phenomenon, it would not be affected by the proportions of carburized to non-carburized material, although the tensile specimens would be affected. For tensile (and impact) tests and fatigue tests, the cracks initiated at different positions. Cracks initiated at the surface of the fatigue specimens, with some secondary cracks found on the sub-surfaces, whereas cracks initiated within the core of tensile and impact (around the notches) specimens. Thus, the decreased impact toughness and UTS of the carburized steel could be attributed to the brittle carbides and oxides that formed during carburizing, resulting in coarse grains (Figures 5–8) allowing for easy crack propagation.

From this work, pack carburizing was shown to be unsuitable for AISI 316L stainless steel, as the process significantly reduced the ductility, ultimate tensile strength, and impact toughness. The plasma and gas carburizing techniques, in contrast, are known to considerably improve mechanical properties.

Conclusions

Surface hardness was unchanged at carburizing temperatures of 450 and 550°C, but increased with increasing temperature above 550°C due to intergranular and intragranular carbide precipitation.

An increase in pack carburizing temperature to 650, 700, or 750°C adversely influenced the mechanical properties of AISI 316L austenitic stainless steel by decreasing the ductility, toughness, tensile strength, and fatigue resistance.

The mode of failure was mostly cleavage, fatigue failure, and ductile dimples, with some secondary cracking from microvoid coalescence.

In summary, the process of pack carburizing at or above 650°C was found to be unsuitable for increasing the fatigue resistance of AISI 316L austenitic stainless steel, and carburizing below 650°C gave no benefit.

Acknowledgements

The authors thank the Department of Science and Technology and the National Research Foundation, South Africa for providing funding for this research. They also thank Mr Richard Couperthwaite of the Advanced Materials Division, Mintek, for help with the SEM imaging and analysis.

References

Agarwal, N., Kahn, H., Avishai, A., Michal, G., Ernst, F., and Heuer, A. H. 2007. Enhanced fatigue resistance in 316L austenitic stainless steel due to low-temperature paraequilibrium carburization. *Acta Materialia*, vol. 55, no. 16. pp. 5572–5580.

Akita, M. and Tokaji, K. 2006. Effect of carburizing on notch fatigue behaviour in AISI 316 austenitic stainless steel. *Surface and Coatings Technology*, vol. 200, no. 20-21. pp. 6073–6078.

ASTM Standards. 2000. Metals Testing Methods and Analytical Procedures. *Metals - Mechanical testing; Elevated and low-temperature tests*, vol. 03.01.

Azar, V., Hashemi, B., and Yazdi, R.M. 2010. The effect of shot peening on fatigue and corrosion behavior of 316L stainless steel in Ringer's solution. *Surface and Coatings Technology*, vol. 204, no. 21-22. pp. 3546–3551.

Bain, E.C. and Griffiths, W.E. 1927. An introduction to the iron-chromium-nickel alloys. *Transactions of the American Institute of Mineral and Metallurgical Engineering*, vol. 75. pp. 166–213.

Bell, T. 2002. Surface engineering of austenitic stainless steel. *Surface Engineering*, vol. 18, no. 6. pp. 415–422.

Berríos, J.A., Teer, D.G., and Puchi-Cabrera, E.S. 2001. Fatigue properties of a 316L stainless steel coated with different TiNx deposits. *Surface and Coatings Technology*, vol. 148, no. 2-3. pp. 179–190.

Berríos-Ortíz, J.A., La Barbera-Sosa, J.G., Teer, D.G., and Puchi-Cabrera, E.S. 2004. Fatigue properties of a 316L stainless steel coated with different ZrN deposits. *Surface and Coatings Technology*, vol. 179, no. 2-3. pp. 145–157.

Ceschini, L. and Minak, G. 2008. Fatigue behaviour of low temperature carburised AISI 316L austenitic stainless steel. *Surface and Coatings Technology*, vol. 202, no. 9. pp. 1778–1784.

Collins, G.A., Hutchings, R., Short, K.T., Tendys, J., Li, X., and Samandi, M. 1995. Nitriding of austenitic stainless steel by plasma immersion ion implantation. *Surface and Coatings Technology*, no. 74-75. pp. 417–424.

Davis, J.R. 1994. ASM Handbook: Carburising and Carbonitriding. ASM International, Materials Park, Ohio:

De Freitas, M., Reis, L., Da Fonte, M., and Li, B. 2011. Effect of steady torsion on fatigue crack initiation and propagation under rotating bending: Multiaxial fatigue and mixed-mode cracking. *Engineering Fracture Mechanics*, vol. 78, no. 5. pp. 826–835.

Fewell, M.P., Mitchell, D.R.G., Priest, J.M., Short, K.T., and Collins, G.A. 2000. The nature of expanded austenite. *Surface and Coatings Technology*, vol. 131, no. 1-3. pp. 300–306.

Fong, C. and Tromans, D. 1988. Stage 1 corrosion fatigue crack crystallography in austenitic stainless steel (316L). *Metallurgical Transactions A*, vol. 19A. pp. 2765–2773.

Gao, N., Brown, M.W., and Miller, K.J. 1995. Crack growth morphology and microstructural changes in 316 stainless steel under creep-fatigue cycling. *Fatigue and Fracture of Engineering Materials and Structures*, vol. 18, no. 12. pp. 1407–1422.

Gelfi, M., La Vecchia, G.M., Lecis, N., and Troglio, S. 2005. Relationship between through-thickness residual stress of CrN-PVD coatings and fatigue nucleation sites. *Surface and Coatings Technology*, vol. 192, no. 2–3. pp. 263–268.

Grosskreutz, J.C. and Waldow, P. 1963. Substructure and fatigue fracture in aluminum. *Acta Metallurgica,* vol. 11, no. 7. pp. 717–724.

Hull, D. 1999. Fractography, Observing, Measuring and Intrepreting Fracture Surface Topography. Cambridge University Press, Cambridge, UK.

James, R.D. 1981. Finite deformation by mechanical twinning. *Archive for Rational Mechanics and Analysis*, vol. 77, no. 2. pp. 143–176.

Jenkins, C.H.M., Bucknall, E.H., Austin, C.R., and Mellor, G.A. 1937. Some alloys for use at high temperatures. Part IV: The constitution of the alloys of nickel, chromium and iron. *Journal of the Iron and Steel Institute*, vol. 136. pp. 187–222.

Jin-Bo, B. and Chen, S.-Y. 1988. Secondary cracking during surface crack growth under tensile fatigue loading. *Engineering Fracture Mechanics*, vol. 30, no. 2. pp. 161–167.

King, J.E. and Cotterill, P.J. 1990. Role of oxides in fatigue crack propagation. *Materials Science and Engineering*, vol. 6. pp. 19–31.

Lampman, S. 1997. Weld Integrity and Performance. ASM International, Materials Park, Ohio.

Liang, J.H., Wang, C.S., Tsai, W.F., and Ai, C.F. 2007. Parametric study of nitrided AISI 304 austenite stainless steel prepared by plasma immersion ion implantation. *Surface and Coatings Technology*, vol. 201, no. 15. pp. 6638–6642.

Liu, C., Bi, Q., Leyland, A., and Matthews, A. 2003. An electrochemical impedance spectroscopy study of the corrosion behaviour of PVD coated steels in 0.5 N NaCl aqueous solution: Part II. *Corrosion Science*, vol. 45, no. 6. pp. 1257–1273.

Liu, P. 2006. Quantitative analysis of multi-phase steels of ferrite and austenite. PhD thesis, Linkoping University.

Lu, K., Lu, L., and Suresh, S. 2009. Strengthening materials by engineering coherent internal boundaries at the nanoscale. *Science*, vol. 324, no. 5925. pp. 349–52.

Lukáš, P. and Kunz, L. 2004. Role of persistent slip bands in fatigue. *Philosophical Magazine*, vol. 84, no. 3-5. pp. 317–330.

Matula, M., Hyspecka, L., Svoboda, M., Vodarek, V., Dagbert, C., Galland, J., Stonawska, Z, and Tuma, L. 2001. Intergranular corrosion of AISI 316L steel. *Materials Characterization*, vol. 46. pp. 203–210.

Mingolo, N., Tschiptschin, A.P., and Pinedo, C.E. 2006. On the formation of expanded austenite during plasma nitriding of an AISI 316L austenitic stainless steel. *Surface and Coatings Technology*, vol. 201, no. 7. pp. 4215–4218.

Renevier, N., Collignon, P., Michel, H., and Czerwiec, T. 1999. Low temperature nitriding of AISI 316L stainless steel and titanium in a low pressure arc discharge. *Surface and Coatings Technology*, vol. 111, no. 2-3. pp. 128–133.

Ritchie, R.O. and Lankford, J. 1986. Small fatigue cracks: A statement of the problem and potential solutions. *Materials Science and Engineering*, vol. 84. pp. 11–16.

Roylance, D. 2001. Introduction to Fracture Mechanics. Massachusetts Institute of Technology.

Samandi, M., Shedden, B.A., Smith, D.I., Collins, G.A., Hutchings, R., and Tendys, J. 1993. Microstructure, corrosion and tribological behaviour of plasma immersion ion-implanted austenitic stainless steel. *Surface and Coatings Technology*, vol. 59, no. 1-3. pp. 261–266.

Shewmon, G.P. 1963. Diffusion in Solids. McGraw Hill, Tokyo.

Tvergaard, V. 2008. Effect of T-stress on crack growth under mixed mode I-III loading. *International Journal of Solids and Structures*, vol. 45, no. 18-19. pp. 5181–5188.

Wei, S., Jinhua, Z., Liujie, X., and Rui. J. 2006. Effects of carbon on microstructures and properties of high vanadium high-speed steel. *Materials and Design*, vol. 27, no. 1. pp. 58–63.

Yang, F., Yin, S.M., Li, S.X., and Zhang, Z.F. 2008. Crack initiation mechanism of extruded AZ31 magnesium alloy in the very high cycle fatigue regime. *Materials Science and Engineering A*, vol. 491, no. 1-2. pp. 131–136.

Yates, J.R. and Mohammed, R.A. 1996. The determination of fatigue crack propagation rates under mixed mode (I+III) loading. *International Journal of Fatigue*, vol. 18, no. 3. pp. 197–203.

Zapffe, C.A. 1949. Stainless Steels. American Society for Metals, Materials Park, Ohio.

Zavattieri, P.D. and Espinosa, H.D. 2001. Grain level analysis of crack initiation and propagation in brittle materials. *Acta Materialia*, vol. 49, no. 20. pp. 4291–4311. ◆